Available online at www.sciencedirect.com
ScienceDirect
Mathematics and Computers in Simulation 181 (2021) 333–350
MATHEMATICS AND COMPUTERS IN SIMULATION
www.elsevier.com/locate/matcom

Original articles

Evaluating the unsteady MHD micropolar fluid flow past stretching/shirking sheet with heat source and thermal radiation: Implementing fourth order predictor–corrector FDM

M.M. Khader[a,b,*], Ram Prakash Sharma[c]

[a] Department of Mathematics and Statistics, College of Science, Imam Mohammad Ibn Saud Islamic University (IMSIU), Riyadh, Saudi Arabia
[b] Department of Mathematics, Faculty of Science, Benha University, Benha, Egypt
[c] Department of Mechanical Engineering, NIT Arunachal Pradesh, Yupia, Papum Pare District, Arunachal Pradesh 791112, India

Received 7 October 2019; received in revised form 23 August 2020; accepted 16 September 2020
Available online 28 September 2020

Abstract

The idea of the current investigation is to analyze the effect of thermal radiation and non-uniform heat source/sink on unsteady MHD micropolar fluid flow past a stretching/shirking sheet. The governing non-linear PDEs are transformed into a set of non-linear coupled ODEs which are then solved numerically by using the fourth order predictor–corrector finite difference method (PC4-FDM). The effect of non-dimensional governing parameters on momentum, angular momentum, energy and mass descriptions is examined and displayed with the aid of their graphical depictions. Also, friction factor, heat and mass transfer rates have been enumerated and shown through tables. Under some special conditions, current outcomes are compared with the existing outcomes to examine the exactness and validity of the current study. An excellent agreement is found with the existing outcomes. Finally, it is observed that velocity increases with an increase in both micro-polar parameter and thermal buoyancy parameter. In addition, for the temperature profiles opposite behavior is observed for increment in both unsteadiness parameter and thermal buoyancy parameter.

Keywords: Non-uniform heat source/sink; Joule heating; MHD; Micropolar fluid; Fourth-order predictor–corrector FDM

1. Introduction

Micropolar fluids that can undergo rotation are those that obey the constitutive equations of the considered non-Newtonian fluid model with a microstructure belonging to a class of fluids with non-symmetrical stress tensor. Physically, these types of fluids represent fluids consisting of randomly oriented particles suspended in a viscous medium. This model of fluid may be applied to explain the flow of liquid crystals, animal blood, colloidal fluids, suspension solutions, etc. The micropolar fluid flow has attracted considerable attention during the last few decades due to its various applications in many industrial applications such as plasma physics, furnace design and nuclear-power plants. Over the past twenty years, a huge number of research activities in the field of micropolar

* Corresponding author at: Department of Mathematics and Statistics, College of Science, Imam Mohammad Ibn Saud Islamic University (IMSIU), Riyadh, Saudi Arabia.
E-mail addresses: mohamed.khader@fsc.bu.edu.eg (M.M. Khader), ramprakash0808@gmail.com (R.P. Sharma).

https://doi.org/10.1016/j.matcom.2020.09.014

fluid flow have been introduced. For micropolar fluid flow that is related to fluid mechanics in microchannels and micromachined fluid systems, several references [35,40,49] are available ranging from purely analytical to experimental techniques. Another important focus of the present work is the role played by the heat generation that may be appear in the important studies [33,34,44]. However, the MHD laminar fluid flow is also encountered in practice, especially in cases where the induced magnetic field is negligible and a high rate transfer is desirable; hence, many investigations [16,21,26,29,36,41,43,45] have been carried out. In this paper, we consider the free convection boundary layer flow of a micropolar fluid above a stretching surface. The related problems in which the temperature of the plate has some prescribed constant value above ambient have been treated by [2,6,61]. Recently, FEM analysis for unsteady mixed convection flow of a micropolar fluid past a permeable shrinking surface has been examined by Gupta et al. [15]. Stagnation-point flow of a micropolar fluid past a stretching surface has been examined by Nazar et al. [39]. Stagnation-point flow of a micropolar fluid past a shrinking surface has been analyzed by Ishak et al. [28]. It has been observed that the results for a shrinking sheet are nonunique. KBM analysis for boundary layer mixed convection flow of a micropolar fluid in the presence of Soret and Dufour effects has been presented by Srinivasacharya and Ram Reddy [52]. Shaw et al. [50] have examined the influence of the homogeneous, heterogeneous reactions in a micropolar fluid flow over a permeable stretching or shrinking surface in a porous medium. Aziz [5] has discussed the influence of viscous dissipation on mixed convection laminar flow and heat transfer characteristic of a micropolar fluid past an exponentially stretching surface. Rashidi et al. [47] have presented HAM analysis for heat transfer behavior of a micropolar fluid in a porous medium under the influence of radiation. Influence of thermal radiation on micropolar fluid flow and heat transfer past a porous shrinking surface has been analyzed by Bhattacharyya et al. [8]. Yacob et al. [54] have discussed melting heat transfer in a steady laminar stagnation-point flow of a micropolar fluid over a stretching/shrinking surface. The MHD boundary layer transient mixed convection flow of a micropolar fluid over an oscillatory moving vertical porous plate in the presence of thermal radiation has been analyzed by Kim and Fedorov [31]. Raptis [46] has studied the boundary layer flow of a micropolar fluid in a porous medium. The FEM analysis for mixed convection micropolar fluid over a porous stretching surface has been analyzed by Bhargava et al. [7]. The boundary layer flow behavior of a micropolar fluid past a stretching surface has been discussed by Desseaux and Kelson [11]. Hsiao [25] has discussed the heat and mass transfer of a boundary layer flow of a micropolar fluid flow in the presence of radiation over a nonlinear stretching surface [3,10,12–14,17–20,22–24,30,32,37,38,42,48,53,55–60,62]. In this work we decided to focus on following problems: the first is to examine influence of the external magnetic field, non-uniform heat generation/absorption and the thermal radiation on the heat transfer and micropolar fluid flow over a stretching permeable surface. The second objective is to explain the mechanisms of viscous dissipation in the fluid flow. The third goal is to provide a novel numerical solution for this physical problem with use fourth order predictor–corrector FDM.

2. Formulation of the problem

Consider an unsteady two-dimensional mixed convection flow of an incompressible boundary layer flow of a MHD micropolar fluid over a permeable stretching/shrinking sheet. At $t < 0$ the fluid is in steady state and at $t \geq 0$, the fluid, heat and mass flows are in unsteady state.

We consider a stretching/shrinking velocity $u_w(x,t) = \frac{ax}{1-et}$, temperature and concentration of the sheet are $T_w(x,t) = T_\infty + \frac{bx}{1-et}$ and $C_w(x,t) = C_\infty + \frac{bx}{1-et}$, where a, b and e are constants. The stretching/shrinking sheet which is taken along the s-axis and y-axis is normal to it (see Fig. 1). The magnetic field of strength B is applied along y-direction. Under the above assumptions, the governing equations of the flow are [1,51]:

$$\frac{\partial u}{\partial x} + \frac{\partial v}{\partial y} = 0, \tag{1}$$

$$\frac{\partial u}{\partial t} + u\frac{\partial u}{\partial x} + v\frac{\partial u}{\partial y} = \left(\frac{\mu+\kappa}{\rho}\right)\frac{\partial^2 u}{\partial y^2} + \left(\frac{\kappa}{\rho}\right)\frac{\partial N}{\partial y} + g\beta(T - T_\infty) + g\beta^*(C - C_\infty) - \frac{\sigma B_0^2}{\rho}u, \tag{2}$$

$$\frac{\partial N}{\partial t} + u\frac{\partial N}{\partial x} + v\frac{\partial N}{\partial y} = \left(\frac{\gamma}{\rho j}\right)\frac{\partial^2 N}{\partial y^2} - \frac{\kappa}{\rho j}\left(2N + \frac{\partial u}{\partial y}\right), \tag{3}$$

$$\frac{\partial T}{\partial t} + u\frac{\partial T}{\partial x} + v\frac{\partial T}{\partial y} = \frac{\kappa}{\rho c_p}\frac{\partial^2 T}{\partial y^2} - \frac{1}{\rho c_p}\frac{\partial q_r}{\partial y} + \left(\frac{\mu+\kappa}{\rho c_p}\right)\left(\frac{\partial u}{\partial y}\right)^2 + \frac{\sigma B^2}{\rho c_p}u^2 + q''', \tag{4}$$

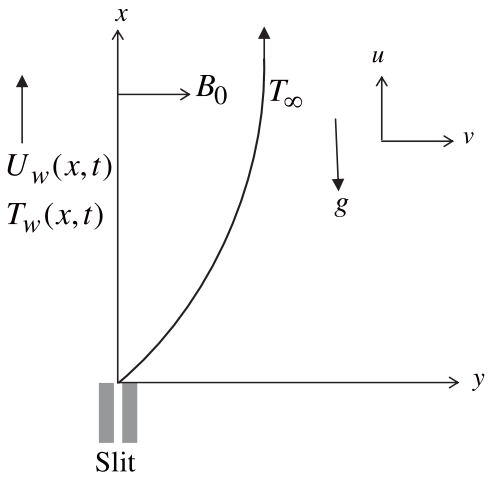

Fig. 1. Coordinate system for the physical model.

$$\frac{\partial C}{\partial t} + u\frac{\partial C}{\partial x} + v\frac{\partial C}{\partial y} = D_m\frac{\partial^2 C}{\partial y^2}. \tag{5}$$

Subject to the boundary conditions:

$$\begin{aligned} &u = \lambda U_m(x,t), \quad v = v_w, \quad N = -\frac{1}{2}\frac{\partial u}{\partial y}, \quad T = T_w(x,t), \quad C = C_w(x,t), \quad \text{at } y = 0, \\ &u \to 0, \quad N \to 0, \quad T \to T_\infty, \quad C \to T_\infty, \quad \text{at } y \to \infty, \end{aligned} \tag{6}$$

where u and v are the velocity components in the x and y directions respectively, ν is the kinematic viscosity, λ is the stretching/shrinking parameter, $\lambda > 0$ for stretching and $\lambda < 0$ for shrinking, v_w is the suction/injection parameter, $v_w > 0$ for suction and $v_w < 0$ for injection, a is positive constant with dimension per time, b is constant with dimension temperature over length, B_0 is the applied magnetic field, C is concentration of the solute, c_p is the specific heat at constant pressure, C_w is the concentration of the solute at the sheet, C_∞ is the concentration of the solute far from the sheet, g is the acceleration due to gravity, κ is the kinematic micro-rotation viscosity, N is the micro-rotation component, β is the coefficient of thermal expansion, β^* is the coefficient of concentration expansion, μ is the coefficient of viscosity, ρ is the density of the fluid, T is the temperature, T_w is the wall temperature of the fluid, T_∞ is the temperature of the fluid far away from the sheet, α is the stretching rate, σ is the electrical conductivity, $\gamma = \left(\mu + \frac{\kappa}{2}\right) j$ is the spin gradient viscosity, j is the micro-inertia density, q_r is the radiative heat flux, D_m is the molecular diffusivity, q''' is the non-uniform heat source/sink and is defined as:

$$q''' = \left(\frac{kU_w(x,t)}{x\nu}\right)(A^*(T_w - T_\infty)f' + B^*(T - T_\infty)), \tag{7}$$

where A^* and B^* are parameters of the space and temperature dependent internal heat source/sink. The positive and negative values of A^* and B^* represents heat source and sink respectively.

Thermal radiation is simulated by using the Rosseland diffusion approximation and, according to this, the radiative heat flux q_r is given by:

$$q_r = -\frac{4\sigma^*}{3k^*}\frac{\partial T^4}{\partial y}, \tag{8}$$

where σ^* is the Stefan–Boltzmann constant and k^* is the Rosseland mean absorption coefficient. It should be noted that, by using the Rosseland approximation, the present analysis is limited to optically thick fluids. If the temperature differences within the flow are sufficiently small, then Eq. (7) can be linearized by expanding T^4 into the Taylor series about T, and neglecting higher-order terms, we get:

$$T^4 \cong 4T_\infty^3 T - 3T_\infty^4. \tag{9}$$

Invoking Eqs. (8) and (9), Eq. (4) can be written as:

$$\frac{\partial T}{\partial t}+u\frac{\partial T}{\partial x}+v\frac{\partial T}{\partial y}=\left(\frac{\kappa}{\rho c_p}+\frac{16T_\infty^3}{3\rho c_p k^*}\right)\frac{\partial^2 T}{\partial y^2}+\left(\frac{\mu+\kappa}{\rho c_p}\right)\left(\frac{\partial u}{\partial y}\right)^2+\frac{\sigma B^2}{\rho c_p}u^2+q'''. \tag{10}$$

In order to obtain similarity solution of the problem, the following non-dimensional variables are introduced:

$$\begin{aligned}&\xi=\sqrt{\frac{a}{\upsilon(1-et)}}y, \qquad \psi=\sqrt{\frac{\upsilon a}{(1-et)}}xf(\xi), \qquad N=\sqrt{\frac{a^3}{\upsilon(1-et)^3}}xh(\xi),\\ &\theta=\frac{T-T_\infty}{T_w-T_\infty}, \qquad \phi=\frac{C-C_\infty}{C_w-C_\infty}, \qquad B=\frac{B_0}{\sqrt{1-et}},\end{aligned} \tag{11}$$

where ξ is the similarity variable and $\psi(x,y)$ is the stream function defined by:

$$u=\frac{\partial\psi}{\partial y}=U_w f'(\xi), \qquad v=-\frac{\partial\psi}{\partial x}=-\sqrt{\frac{\upsilon a}{(1-et)}}f(\xi),$$

which identically satisfies Eq. (1). Similarity variables (11), Eqs. (2), (3), (9) and (5) are used to obtain the following set of ordinary differential equations:

$$(1+K)f'''+ff''-f'^2-\tau\left(f'+\frac{1}{2}\xi f''\right)+Kh'+\delta\theta+\delta^*\phi-Mf'=0, \tag{12}$$

$$\left(1+\frac{K}{2}\right)h''+\begin{vmatrix}f & f'\\ h & h'\end{vmatrix}-\tau\left(\frac{3}{2}h+\frac{1}{2}\xi h'\right)-K(2h+f'')=0, \tag{13}$$

$$\left(1+\frac{4}{3}R\right)\theta''+Pr\begin{vmatrix}f & f'\\ \theta & \theta'\end{vmatrix}-Pr\,\tau\left(2\theta+\frac{1}{2}\xi\theta'\right)+PrEc(1+K)f''^2+PrMEcf'^2+A^*f'+B^*\theta=0, \tag{14}$$

$$\phi''+Sc\begin{vmatrix}f & f'\\ \phi & \phi'\end{vmatrix}-Sc\,\tau\left(\phi+\frac{1}{2}\xi\phi'\right)=0. \tag{15}$$

The corresponding boundary conditions are

$$\begin{aligned}&f(0)=S, \qquad f'(0)=\lambda, \qquad h(0)=-\frac{1}{2}f''(0), \qquad \theta(0)=1, \qquad \phi(0)=1,\\ &f'(\infty)=0, \qquad h(\infty)=0, \qquad \theta(\infty)=0, \qquad \phi(\infty)=0,\end{aligned} \tag{16}$$

where the notation primes denote differentiation with respect to ξ and the parameters are defined as: unsteadiness parameter, $\tau=\frac{a}{e}$, micropolar parameter $K=\frac{\kappa}{\mu}$, magnetic field parameter $M=\frac{\sigma B_0^2}{a\rho}$, thermal Grashof number, $Gr=\frac{g\beta(T_w-T_\infty)x^2}{aU_w}$, thermal buoyancy parameter $\delta=\frac{Gr}{(Re)^2}$, solutal Grashof number, $Gc=\frac{g\beta^*(C_w-C_\infty)x^2}{\upsilon U_w}$, concentration buoyancy parameter $\delta^*=\frac{Gc}{(Re)^2}$, suction/injection parameter, $S>0$ for suction and $S<0$ for injection $S=-\frac{v_w}{\sqrt{a\upsilon}}$ Prandtl number $Pr=\frac{\upsilon}{\alpha}$, Eckert number $Ec=\frac{U_w^2}{c_p(T_w-T_\infty)}$, thermal radiation parameter $R=\frac{4\sigma T_\infty^3}{\kappa k^*}$, and Schmidt number $Sc=\frac{\upsilon}{D_m}$.

Also the quantities of physical interest in this problem are the local skin friction factor, couple stress factor, local rate of heat and mass transfer coefficients, which are defined by

$$C_{fx}=\frac{\tau_w|_{y=0}}{\rho U_w^2}=2(1+K)\sqrt{Re_x}f''(0), \tag{17}$$

$$C_{sx}=\frac{\gamma a U_w}{(1-et)}h'(0), \tag{18}$$

$$Nu_x=-\frac{x}{(T_w-T_\infty)}\frac{\partial T}{\partial y}\Big|_{y=0}=-\sqrt{Re_x}\theta'(0), \tag{19}$$

$$Sh_x=-\frac{x}{(C_w-C_\infty)}\frac{\partial C}{\partial y}\Big|_{y=0}=-\sqrt{Re_x}\phi'(0), \tag{20}$$

where $Re_x=\frac{U_w x}{\upsilon}$ is the Reynolds number.

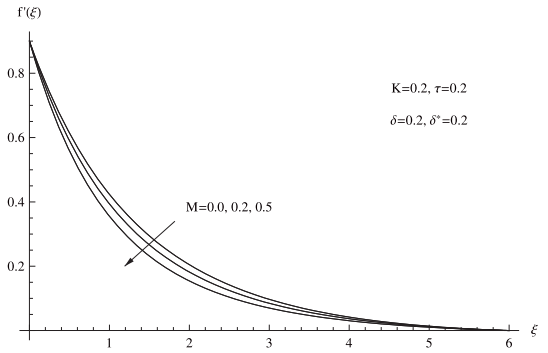

(a) Velocity for changing M.

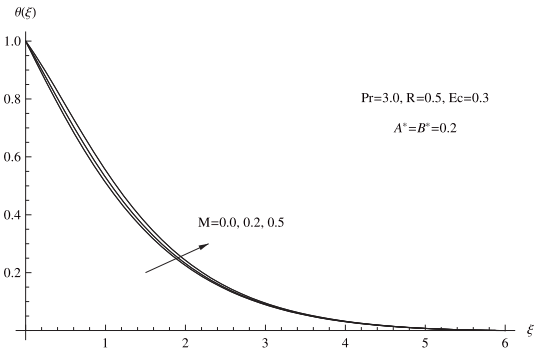

(b) Temperature for changing M.

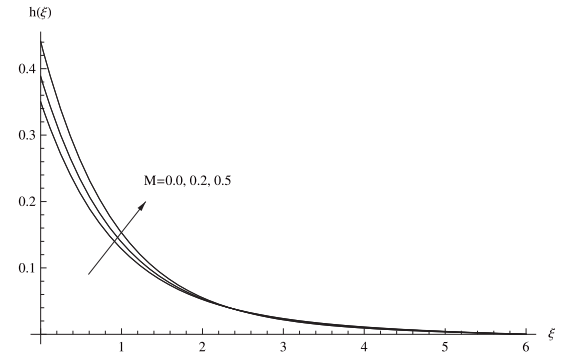

(c) Micro-rotation for changing M.

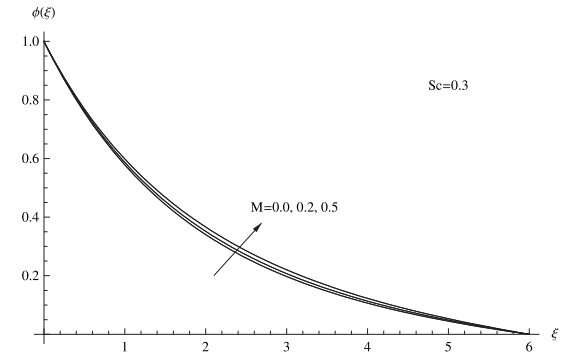

(d) Concentration for changing M.

Fig. 2.

3. Numerical scheme of the proposed problem

In this section, we will implement the proposed method (PC4-FDM) [9] to solve numerically the problem understudy. In this work, we use this method because it is not only an explicit method without requiring for solving any matrix-equation but also it is unconditionally convergent. It is known that in FDM, the space solution's domain $[0, \xi_\infty]$ is divided into some subintervals. We use the symbols $\hbar > 0$ to be the grid step, $\hbar = \xi_\infty / N$ with $\xi_i = i\,\hbar$ for $i = 0, 1, \ldots, N$ [27] and will define $y_i = y(\xi_i)$. Now, to achieve this aim we will implement the proposed numerical method to solve the presented system of ODEs (12)–(16) by introducing the following steps:

1. Use the auxiliary parameters $f' = \mathbb{F}$, $h' = \mathbb{H}$, $\theta' = \Theta$, and $\phi' = \Phi$ to reduce the system (12)–(15) in the following form:

$$f' = \mathbb{F}, \tag{21}$$

$$h' = \mathbb{H}, \tag{22}$$

$$\theta' = \Theta, \tag{23}$$

$$\phi' = \Phi, \tag{24}$$

$$\mathbb{F}'' + (1+K)^{-1}(f\mathbb{F}' - \mathbb{F}^2) - \tau(1+K)^{-1}(\mathbb{F} + 0.5\xi\mathbb{F}') + (1+K)^{-1}(K\mathbb{H} + \delta\theta + \delta^*\phi - M\mathbb{F}) = 0, \tag{25}$$

$$\mathbb{H}' + (1+0.5K)^{-1}(f\mathbb{H} - \mathbb{F}h) - \tau(1+0.5K)^{-1}(1.5h + 0.5\xi\mathbb{H}) - K(1+0.5K)^{-1}(2h + \mathbb{F}') = 0, \tag{26}$$

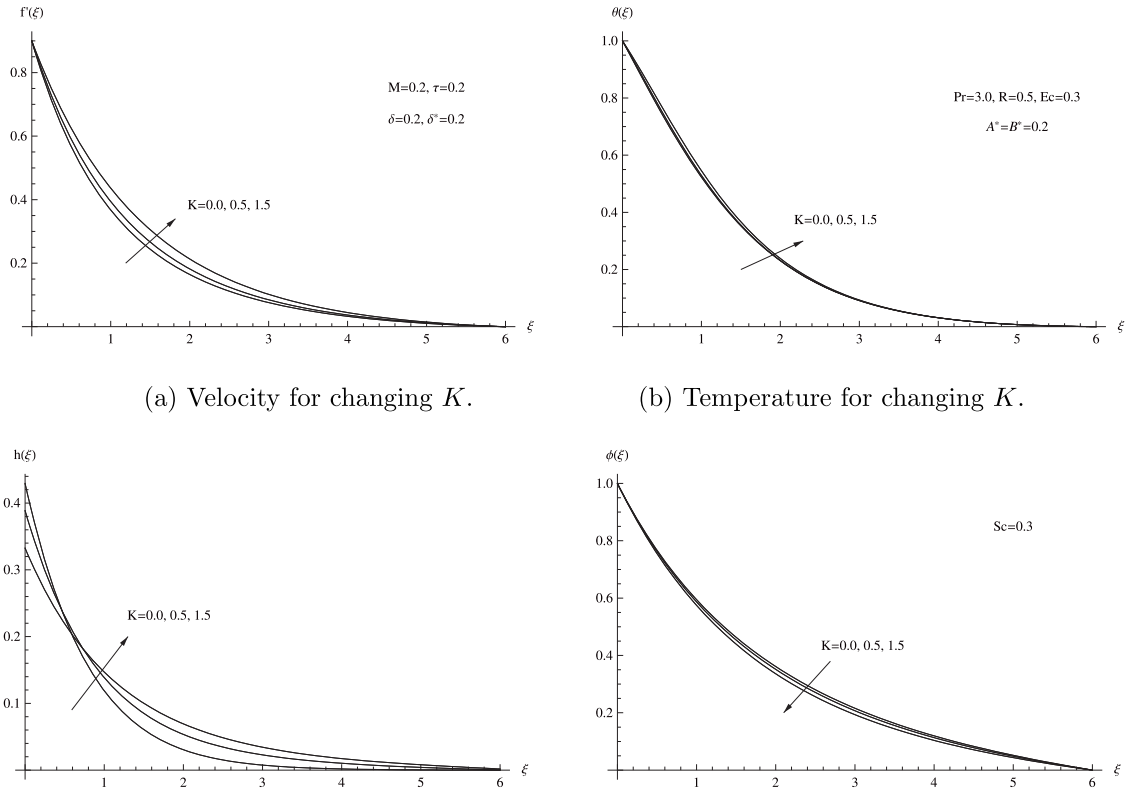

(a) Velocity for changing K. (b) Temperature for changing K.

(c) Micro-rotation for changing K. (d) Concentration for changing K.

Fig. 3.

$$\Theta' + Pr(1+\frac{4}{3}R)^{-1}(f\Theta - \mathbb{F}\theta) - Pr\,\tau(1+\frac{4}{3}R)^{-1}(\theta + 0.5\xi\Theta) + PrEc(1+K)(1+\frac{4}{3}R)^{-1}\mathbb{F}'^2 + (1+\frac{4}{3}R)^{-1}(PrMEc\mathbb{F}^2 + A^*\mathbb{F} + B^*\theta) = 0, \tag{27}$$

$$\Phi' + Sc(f\Phi - \mathbb{F}\phi) - Sc\,\tau(\phi + 0.5\xi\Phi) = 0, \tag{28}$$

with boundary conditions:

$$f(0) = S, \quad \mathbb{F}(0) = \lambda, \quad h(0) = -0.5\mathbb{F}'(0), \quad \theta(0) = 1, \quad \phi(0) = 1, \quad \mathbb{F}(\infty) = 0, \quad h(\infty) = 0, \quad \theta(\infty) = 0, \quad \phi(\infty) = 0. \tag{29}$$

2. Use the approximate formulae of the first and second order derivatives which are defined as follows:

$$Dg_\hbar = \frac{1}{\hbar}\left(\nabla - \frac{1}{2}\nabla^2 - \frac{1}{3!}\nabla^3 - \cdots\right)g_{\hbar+1}, \quad D^2 g_\hbar = \frac{1}{\hbar^2}\left(\nabla^2 - \frac{1}{2}\nabla^4 - \frac{1}{3!}\nabla^5 - \cdots\right)g_{\hbar+1}, \tag{30}$$

where D is the derivative operator and ∇ is the backward operator. So, the system (21)–(28) can be reduced to a system of algebraic equations in the following form [4]:

$$\frac{1}{\hbar}\left(\frac{1}{4}f_{i+1} + \frac{5}{6}f_i - \frac{3}{2}f_{i-1} + \frac{1}{2}f_{i-2} - \frac{1}{12}f_{i-3}\right) = \mathbb{F}_i, \tag{31}$$

$$\frac{1}{\hbar}\left(\frac{1}{4}h_{i+1} + \frac{5}{6}h_i - \frac{3}{2}h_{i-1} + \frac{1}{2}h_{i-2} - \frac{1}{12}h_{i-3}\right) = \mathbb{H}_i, \tag{32}$$

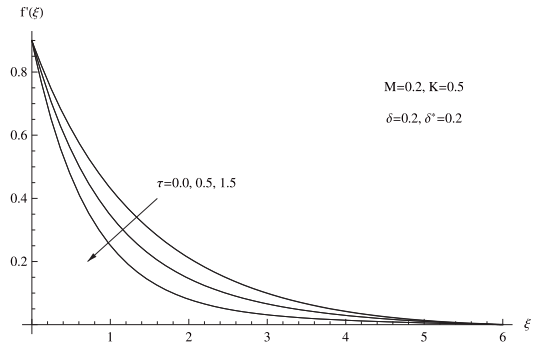

(a) Velocity for changing τ.

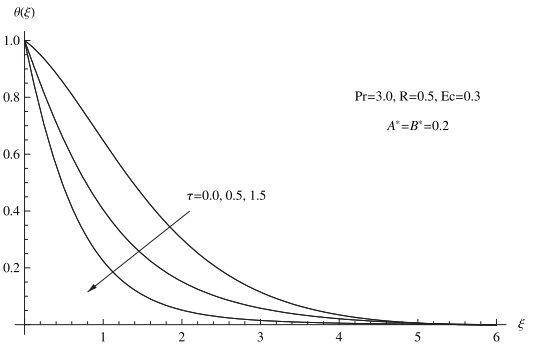

(b) Temperature for changing τ.

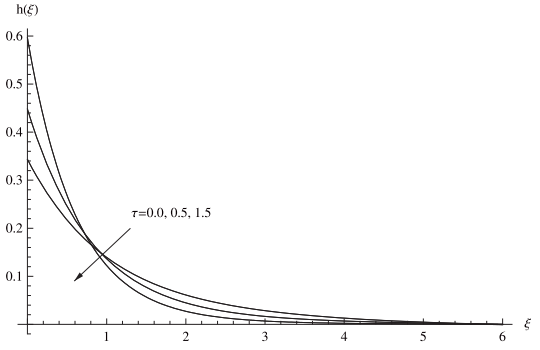

(c) Micro-rotation for changing τ.

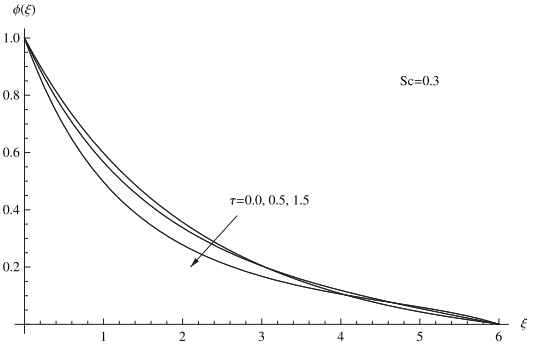

(d) Concentration for changing τ.

Fig. 4.

$$\frac{1}{\hbar}\left(\frac{1}{4}\theta_{i+1}+\frac{5}{6}\theta_i-\frac{3}{2}\theta_{i-1}+\frac{1}{2}\theta_{i-2}-\frac{1}{12}\theta_{i-3}\right)=\Theta_i, \tag{33}$$

$$\frac{1}{\hbar}\left(\frac{1}{4}\phi_{i+1}+\frac{5}{6}\phi_i-\frac{3}{2}\phi_{i-1}+\frac{1}{2}\phi_{i-2}-\frac{1}{12}\phi_{i-3}\right)=\Phi_i, \tag{34}$$

$$\begin{aligned}&\frac{1}{\hbar^2}\left(\frac{5}{6}\mathbb{F}_{i+1}+\frac{5}{4}\mathbb{F}_i-\frac{1}{3}\mathbb{F}_{i-1}+\frac{7}{6}\mathbb{F}_{i-2}-\frac{1}{2}\mathbb{F}_{i-3}+\frac{1}{12}\mathbb{F}_{i-4}\right)\\&\quad+\frac{f_i}{\hbar(1+K)}\left(\frac{1}{4}\mathbb{F}_{i+1}+\frac{5}{6}\mathbb{F}_i-\frac{3}{2}\mathbb{F}_{i-1}+\frac{1}{2}\mathbb{F}_{i-2}-\frac{1}{12}\mathbb{F}_{i-3}\right)\\&\quad-\frac{0.5\tau\xi_i}{\hbar(1+K)}\left(\frac{1}{4}\mathbb{F}_{i+1}+\frac{5}{6}\mathbb{F}_i-\frac{3}{2}\mathbb{F}_{i-1}+\frac{1}{2}\mathbb{F}_{i-2}-\frac{1}{12}\mathbb{F}_{i-3}\right)\\&\quad-(1+K)^{-1}\left(\mathbb{F}_i^2+\tau\mathbb{F}_i-(K\mathbb{H}_i+\delta\theta_i+\delta^*\phi_i-M\mathbb{F}_i)\right)=0,\end{aligned} \tag{35}$$

$$\begin{aligned}&\frac{1}{\hbar}\left(\frac{1}{4}\mathbb{H}_{i+1}+\frac{5}{6}\mathbb{H}_i-\frac{3}{2}\mathbb{H}_{i-1}+\frac{1}{2}\mathbb{H}_{i-2}-\frac{1}{12}\mathbb{H}_{i-3}\right)\\&\quad-\frac{K}{\hbar(1+0.5K)}\left(\frac{1}{4}\mathbb{F}_{i+1}+\frac{5}{6}\mathbb{F}_i-\frac{3}{2}\mathbb{F}_{i-1}+\frac{1}{2}\mathbb{F}_{i-2}-\frac{1}{12}\mathbb{F}_{i-3}\right)\\&\quad+(1+0.5K)^{-1}\left(f_i\mathbb{H}_i-\mathbb{F}_ih_i-\tau(1.5h_i+0.5\xi_i\mathbb{H}_i)-2Kh_i\right)=0,\end{aligned} \tag{36}$$

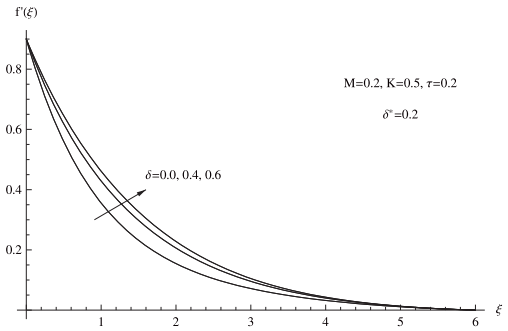

(a) Velocity for changing δ.

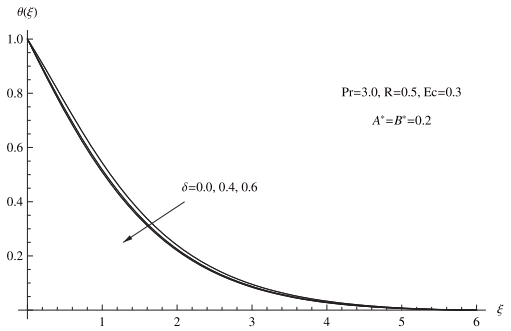

(b) Temperature for changing δ.

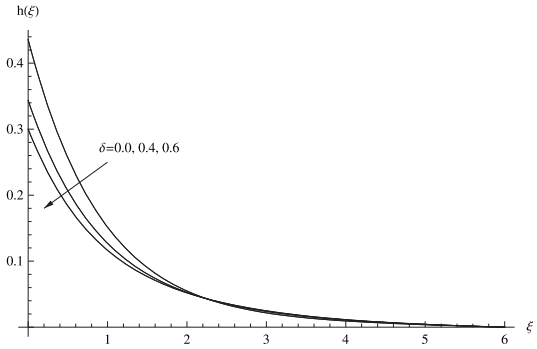

(c) Micro-rotation for changing δ.

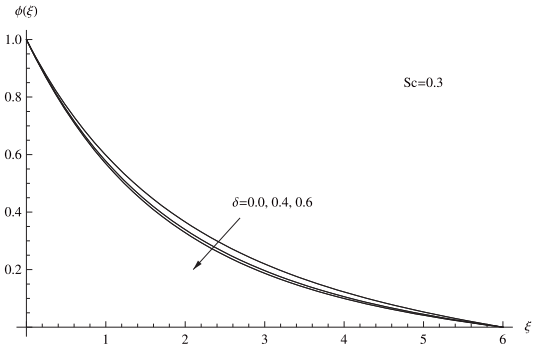

(d) Concentration for changing δ.

Fig. 5.

$$\frac{1}{\hbar}\left(\frac{1}{4}\Theta_{i+1}+\frac{5}{6}\Theta_i-\frac{3}{2}\Theta_{i-1}+\frac{1}{2}\Theta_{i-2}-\frac{1}{12}\Theta_{i-3}\right)$$
$$+\frac{Pr\,Ec(1+K)}{\hbar^2}\left(1+\frac{4}{3}R\right)^{-1}\left(\frac{1}{4}\mathbb{F}_{i+1}+\frac{5}{6}\mathbb{F}i-\frac{3}{2}\mathbb{F}_{i-1}+\frac{1}{2}\mathbb{F}_{i-2}-\frac{1}{12}\mathbb{F}_{i-3}\right)^2 \tag{37}$$
$$+\left(1+\frac{4}{3}R\right)^{-1}\left[Pr(f_i\Theta_i-\mathbb{F}_i\theta_i)-Pr\,\tau(\theta_i+0.5\xi_i\Theta_i)+PrMEc\mathbb{F}_i^2+A^*\mathbb{F}_i+B^*\theta_i\right]=0,$$
$$\frac{1}{\hbar}\left(\frac{1}{4}\Phi_{i+1}+\frac{5}{6}\Phi_i-\frac{3}{2}\Phi_{i-1}+\frac{1}{2}\Phi_{i-2}-\frac{1}{12}\Phi_{i-3}\right)+Sc\,(f_i\Phi_i-\mathbb{F}_i\phi_i)-Sc\,\tau\,(\phi_i+0.5\xi_i\Phi_i)=0. \tag{38}$$

3. Solve the system (31)–(38) explicitly for f_{i+1}, h_{i+1}, θ_{i+1}, ϕ_{i+1}, $\mathbb{F}_{i+1}$, $\mathbb{H}_{i+1}$, Θ_{i+1} and Φ_{i+1}; i.e., by using the subscript s for the predicted values, the predicting values of the solution $(f^{(s)}, h^{(s)}, \theta^{(s)}, \phi^{(s)}, \mathbb{F}^{(s)}, \mathbb{H}^{(s)}, \Theta^{(s)}, \Phi^{(s)})$ of this system take the following form:

$$f_{i+1}^{(s)}=\frac{1}{3}(-10f_i+18f_{i-1}-6f_{i-2}+f_{i-3}+12\hbar\mathbb{F}_i), \tag{39}$$

$$h_{i+1}^{(s)}=\frac{1}{3}(-10h_i+18h_{i-1}-6h_{i-2}+h_{i-3}+12\hbar\mathbb{H}_i), \tag{40}$$

$$\theta_{i+1}^{(s)}=\frac{1}{3}(-10\theta_i+18\theta_{i-1}-6\theta_{i-2}+\theta_{i-3}+12\hbar\Theta_i), \tag{41}$$

$$\phi_{i+1}^{(s)}=\frac{1}{3}(-10\phi_i+18\phi_{i-1}-6\phi_{i-2}+\phi_{i-3}+12\hbar\Phi_i), \tag{42}$$

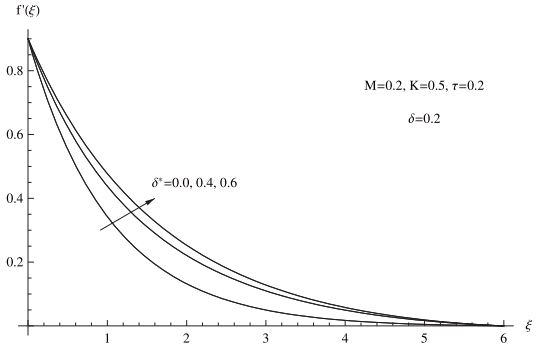

(a) Velocity for changing δ^*.

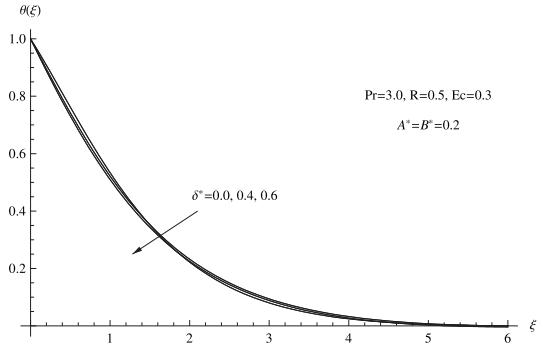

(b) Temperature for changing δ^*.

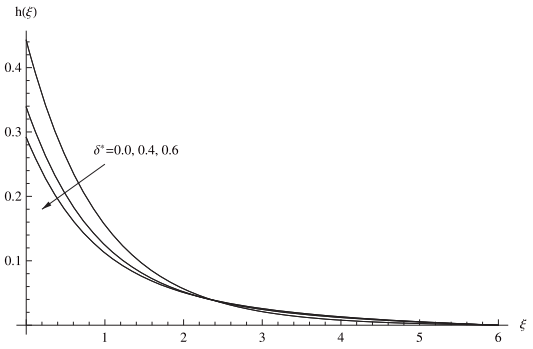

(c) Micro-rotation for changing δ^*.

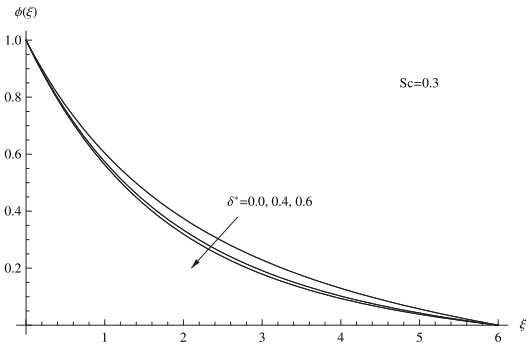

(d) Concentration for changing δ^*.

Fig. 6.

$$\mathbb{F}_{i+1}^{(s)} = \Big(20(1+K)+6\hbar f_i - 3\hbar\tau\xi_i\Big)^{-1}\Big[-\Big(30(1+K)+20f_i\hbar - 10\hbar\tau\xi_i - 24\hbar^2(\tau+M)\Big)\mathbb{F}_i + \Big(8(1+K)+36f_i\hbar - 18\hbar\tau\xi_i\Big)\mathbb{F}_{i-1} - \Big(28(1+K)+12f_i\hbar - 6\hbar\tau\xi_i\Big)\mathbb{F}_{i-2} + \Big(12(1+K)+2f_i\hbar - \hbar\tau\xi_i\Big)\mathbb{F}_{i-3} + 2(1+K)\mathbb{F}_{i-4} + 24\hbar^2\Big(\mathbb{F}_i^2 - K\mathbb{H}_i - \delta\theta_i - \delta^*\phi_i\Big)\Big], \tag{43}$$

$$\mathbb{H}_{i+1}^{(s)} = \frac{1}{3}\Big[-\Big(10+12\hbar\Big(1+0.5K\Big)^{-1}\Big(f_i - 0.5\tau\xi_i\Big)\Big)\mathbb{H}_i + 18\mathbb{H}_{i-1} - 6\mathbb{H}_{i-2} + \mathbb{H}_{i-3} + \Big(1+0.5K\Big)^{-1}\cdot \Big(K\Big(3\mathbb{F}_{i+1} + 10\mathbb{F}_i - 18\mathbb{F}_{i-1} + 6\mathbb{F}_{i-2} - \mathbb{F}_{i-3}\Big) + 12\hbar\Big(\mathbb{F}_i + 1.5\tau + 2K\Big)h_i\Big)\Big], \tag{44}$$

$$\Theta_{i+1}^{(s)} = \frac{1}{3\hbar}\Big[-\Big(10\hbar + 12\hbar^2\Big(1+\frac{4}{3}R\Big)^{-1}Pr\Big(f_i - 0.5\tau\xi_i\Big)\Big)\Theta_i + 18\hbar\Theta_{i-1} - 6\hbar\Theta_{i-2} + \hbar\Theta_{i-3} - 12Pr\,Ec(1+K)\Big(1+\frac{4}{3}R\Big)^{-1}\Big(\frac{1}{4}\mathbb{F}_{i+1} + \frac{5}{6}\mathbb{F}_i - \frac{3}{2}\mathbb{F}_{i-1} + \frac{1}{2}\mathbb{F}_{i-2} - \frac{1}{12}\mathbb{F}_{i-3}\Big)^2 + 12\hbar^2\Big(1+\frac{4}{3}R\Big)^{-1}\Big(Pr\theta_i(\mathbb{F}_i+\tau) - PrMEc\mathbb{F}_i^2 - A^*\mathbb{F}_i - B^*\theta_i\Big)\Big], \tag{45}$$

$$\Phi_{i+1}^{(s)} = \frac{1}{3}\Big[-\Big(10 - 6\hbar\tau Sc\xi_i + 12\hbar Scf_i\Big)\Phi_i + 18\Phi_{i-1} - 6\Phi_{i-2} + \Phi_{i-3} + 12\hbar\phi_i Sc\Big(\tau + \mathbb{F}_i\Big)\Big]. \tag{46}$$

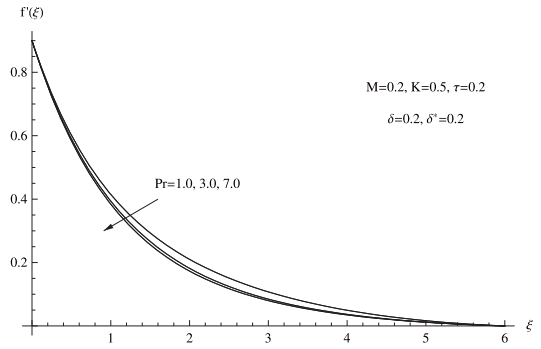

(a) Velocity for changing Pr.

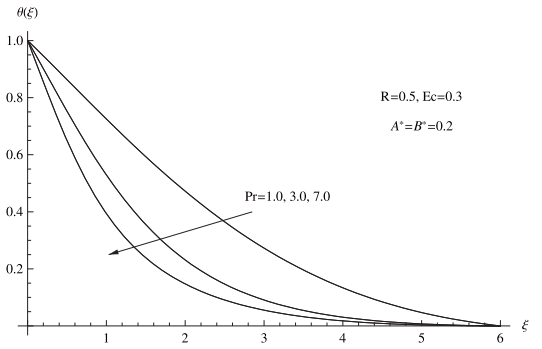

(b) Temperature for changing Pr.

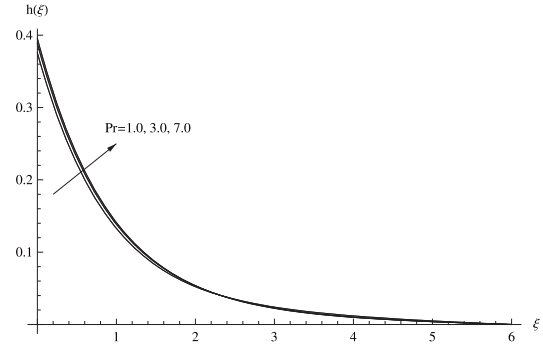

(c) Micro-rotation for changing Pr.

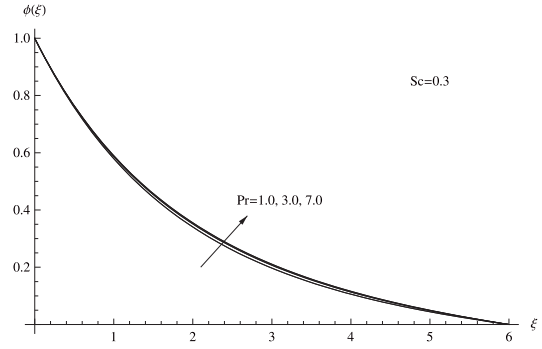

(d) Concentration for changing Pr.

Fig. 7.

4. Use the following operators:

$$Dg_\hbar = \frac{1}{\hbar}\left(\nabla + \frac{1}{2}\nabla^2 + \frac{1}{3}\nabla^3 + \frac{1}{4}\nabla^4 + \cdots\right) g_\hbar, \quad D^2 g_\hbar = \frac{1}{\hbar^2}\left(\nabla^2 + \nabla^3 + \frac{11}{12}\nabla^4 + \frac{5}{6}\nabla^5 + \cdots\right) g_\hbar, \tag{47}$$

to obtain the correct values of the variables which **were** defined in (39)–(46) which take the following form:

$$f_{i+1} = \frac{1}{25}(48 f_i - 36 f_{i-1} + 16 f_{i-2} - 3 f_{i-3} + 12\hbar \mathbb{F}^{(s)}_{i+1}), \tag{48}$$

$$h_{i+1} = \frac{1}{25}(48 h_i - 36 h_{i-1} + 16 h_{i-2} - 3 h_{i-3} + 12\hbar \mathbb{H}^{(s)}_{i+1}), \tag{49}$$

$$\theta_{i+1} = \frac{1}{25}(48\theta_i - 36\theta_{i-1} + 16\theta_{i-2} - 3\theta_{i-3} + 12\hbar\, \Theta^{(s)}_{i+1}), \tag{50}$$

$$\phi_{i+1} = \frac{1}{25}(48\phi_i - 36\phi_{i-1} + 16\phi_{i-2} - 3\phi_{i-3} + 12\hbar\, \Phi^{(s)}_{i+1}), \tag{51}$$

$$\begin{aligned}\mathbb{F}_{i+1} = \Big(20(1+K) + 50\hbar f_i - \hbar\tau\xi_i\Big)^{-1} \Big[&-\Big(30(1+K) - 96 f_i\hbar - 48\hbar\tau\xi_i - 24\hbar^2(\tau + M)\Big)\mathbb{F}_i \\ &+ \Big(8(1+K) - 72 f_i\hbar + 36\hbar\tau\xi_i\Big)\mathbb{F}_{i-1} - \Big(28(1+K) - 32 f_i\hbar + 16\hbar\tau\xi_i\Big)\mathbb{F}_{i-2} \\ &+ \Big(12(1+K) - 6 f_i\hbar + 3\hbar\tau\xi_i\Big)\mathbb{F}_{i-3} + 2(1+K)\mathbb{F}_{i-4} + 24\hbar^2\Big(\mathbb{F}_i^2 - K\mathbb{H}_i - \delta\theta_i - \delta^*\phi_i\Big)\Big],\end{aligned} \tag{52}$$

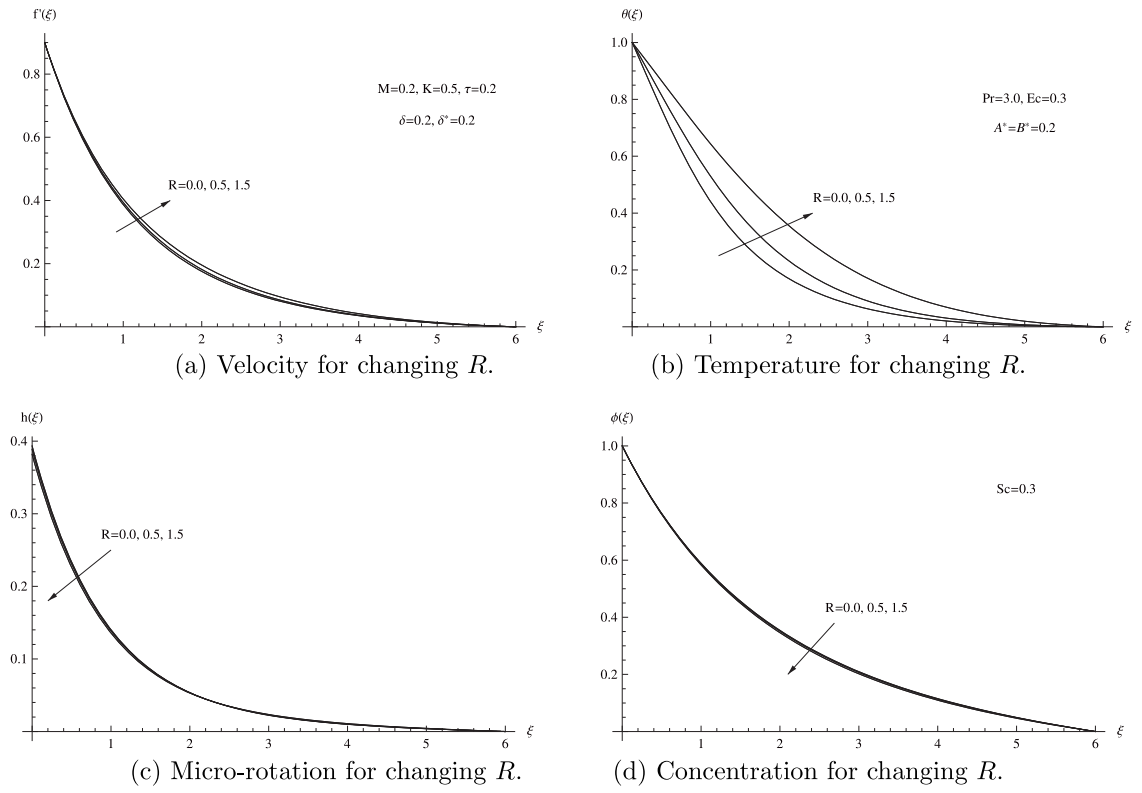

(a) Velocity for changing R. (b) Temperature for changing R.

(c) Micro-rotation for changing R. (d) Concentration for changing R.

Fig. 8.

$$\mathbb{H}_{i+1} = \frac{1}{25}\Big[\Big(48 - 12\hbar\Big(1+0.5K\Big)^{-1}\Big(f_i - 0.5\tau\xi_i\Big)\Big)\mathbb{H}_i - 36\mathbb{H}_{i-1} + 16\mathbb{H}_{i-2} - 3\mathbb{H}_{i-3} + \Big(1+0.5K\Big)^{-1}\cdot \Big(K\Big(25\mathbb{F}_{i+1} - 48\mathbb{F}_i + 36\mathbb{F}_{i-1} - 16\mathbb{F}_{i-2} + 3\mathbb{F}_{i-3}\Big) + 12\hbar\Big(\mathbb{F}_i + 1.5\tau + 2K\Big)h_i\Big)\Big], \tag{53}$$

$$\begin{aligned}\Theta_{i+1} = \frac{1}{25\hbar}\Big[&\Big(48\hbar - 12\hbar^2\Big(1+\frac{4}{3}R\Big)^{-1}Pr\Big(f_i - 0.5\tau\xi_i\Big)\Big)\Theta_i - 36\hbar\,\Theta_{i-1} + 16\hbar\,\Theta_{i-2} - 3\hbar\,\Theta_{i-3}\\ &- 12Pr\,Ec(1+K)\Big(1+\frac{4}{3}R\Big)^{-1}\Big(\frac{25}{12}\mathbb{F}_{i+1} - 4\mathbb{F}_i + 3\mathbb{F}_{i-1} - \frac{4}{3}\mathbb{F}_{i-2} + \frac{1}{4}\mathbb{F}_{i-3}\Big)^2\\ &+ 12\hbar^2\Big(1+\frac{4}{3}R\Big)^{-1}\Big(Pr\theta_i(\mathbb{F}_i+\tau) - PrMEc\mathbb{F}_i^2 - A^*\mathbb{F}_i - B^*\theta_i\Big)\Big],\end{aligned} \tag{54}$$

$$\Phi_{i+1} = \frac{1}{25}\Big[\Big(48 + 12\hbar\tau Sc\xi_i - 12\hbar Scf_i\Big)\Phi_i - 36\,\Phi_{i-1} + 16\,\Phi_{i-2} - 3\,\Phi_{i-3} + 12\hbar\phi_i Sc\Big(\tau + \mathbb{F}_i\Big)\Big]. \tag{55}$$

Here, we apply the PC4-FDM for obtaining the values of f, f', f'', h, h', θ, θ', ϕ and ϕ' at some particular points based to their values at the previous five mesh points. Since the values of f, f', h, θ and ϕ are given at 0, but the values of f', h, θ and ϕ are given at ∞, the proposed system (12)–(15) can be considered as a BVP. Therefore, we can solve these equations by changing the initial guess of f'', h', θ' and ϕ' so that the boundary conditions at ∞ are satisfied. Let us assume that the values of the initial guess of f'', h', θ' and ϕ' are defined as follows:

$$f''(0) = \ell_1, \qquad h'(0) = \ell_2, \qquad \theta'(0) = \ell_3, \qquad \phi'(0) = \ell_4. \tag{56}$$

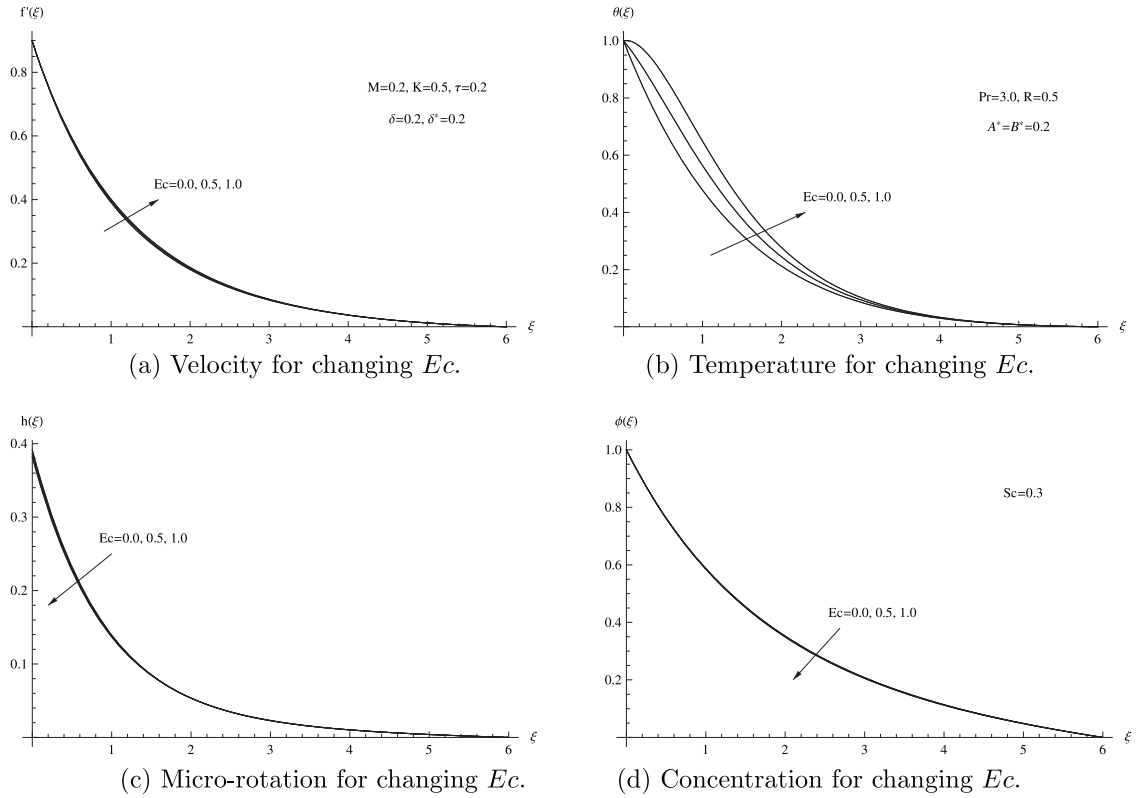

(a) Velocity for changing Ec. (b) Temperature for changing Ec.

(c) Micro-rotation for changing Ec. (d) Concentration for changing Ec.

Fig. 9.

The values of f, h, θ, ϕ, $\mathbb{F}$, $\mathbb{H}$, Θ, and Φ at five extra nodes are needed to start the solution of the obtained equations. So, we can find the values of these parameters in $\xi = \pm h\xi = \pm 2h\xi$ by applying the Taylor series. Since the Taylor series for expansion of f, h, θ and ϕ around $\xi = 0$ takes the following formulae:

$$f(\xi) = \sum_{j=0}^{5} a_j \xi^j, \qquad h(\xi) = \sum_{j=0}^{5} b_j \xi^j, \qquad \theta(\xi) = \sum_{j=0}^{5} c_j \xi^j, \qquad \phi(\xi) = \sum_{j=0}^{5} d_j \xi^j, \tag{57}$$

where a_j, b_j, c_j and d_j are constants and should be obtained by using the boundary values of f, h, θ, ϕ, $\mathbb{F}$, $\mathbb{H}$, Θ, and Φ at $\xi = 0$. Henceforth, some of these constants $a_0, a_1, a_2, b_0, b_1, c_0, c_1, d_0$ and d_1 are obtained on the basis of boundary values of parameters at $\xi = 0$ and others are obtained by using (12)–(15).

4. Results and discussion

For validation of the numerical method that obtained after using fourth order predictor–corrector FDM, we compare our results with those reported by Abd El-Aziz [1] and Singh and Kumar [51] as shown in following Table, and they are found to be in excellent agreement (see Table 1).

The numerical results of the parametric study are introduced with the help of graphical illustrations. Fig. 2(a, b, c, d) are plotted to visualize the characteristics of magnetic parameter M on the micro-polar fluid velocity, temperature, angular momentum and concentration profiles respectively. It is manifest from these figures that the micro-polar fluid temperature, angular momentum and concentration profiles enhance with the augmented values of magnetic parameter while the reverse trend is observed for velocity profile. It is also observed from these figures that the boundary layer thickness for small magnetic parameter is thicker than that of great magnetic parameter. Physically, an addition in magnetic parameter produces higher Lorentz force (resistive force) which has the trademark to change over some kinetic energy into heat energy.

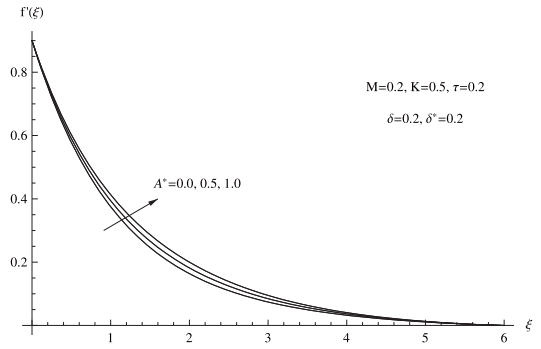

(a) Velocity for changing A^*.

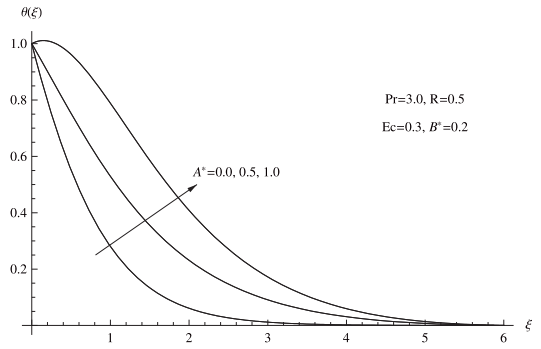

(b) Temperature for changing A^*.

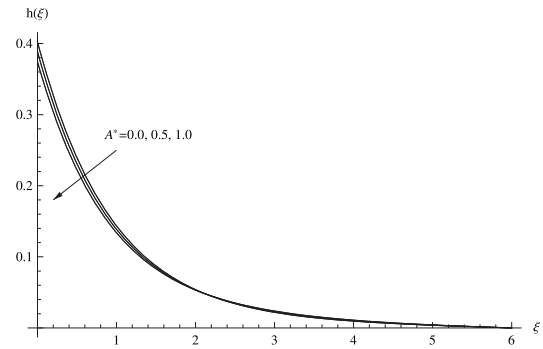

(c) Micro-rotation for changing A^*.

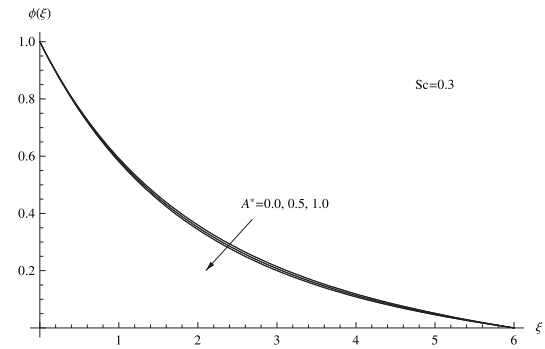

(d) Concentration for changing A^*.

Fig. 10.

Table 1
Comparison of $-\theta'(0)$ for different values of τ and δ when $M = R = Ec = K = A^* = B^* = \delta^* = 0$ and $Pr = 1$.

τ	δ	Abd El-Aziz [1]	Singh and Kumar [51]	Present study
0.0	0.0	1.00000000	1.00000000	1.00000000
0.0	1.0	1.08727816	1.08727818	1.08727812
0.0	2.0	1.14233927	1.14233928	1.14233924
0.0	3.0	1.18529030	1.18529032	1.18529028
1.0	0.0	1.68199254	1.68199255	1.68199253
1.0	1.0	1.70391279	1.70391281	1.70391276

The features of micro-polar fluid velocity, temperature, angular momentum and concentration are presented through Fig. 3(a, b, c, d). It is estimated from these sketches that the micro-polar liquid velocity, temperature and angular momentum profiles are enhanced with the boost values of micro-polar parameter K while the reverse trend is observed for concentration profile. Physically, increasing the micro-polar parameter K causes higher acceleration to the micro-polar fluid flow which, in turn, increases both the velocity motion and the fluid temperature while it causes a decrease in the concentration profiles.

Fig. 4(a, b, c, d) are drafted to deliberate the variations in the micropolar liquid velocity, temperature, angular momentum and concentration distributions under the influence of the unsteadiness parameter τ. It can be perceived from these sketches that the micropolar liquid velocity, temperature, angular momentum and concentration distributions reduce for an escalation in the unsteadiness parameter. Moreover, it is also found that, increasing the unsteadiness parameter τ leads to a decrease in both momentum and thermal boundary layer thickness.

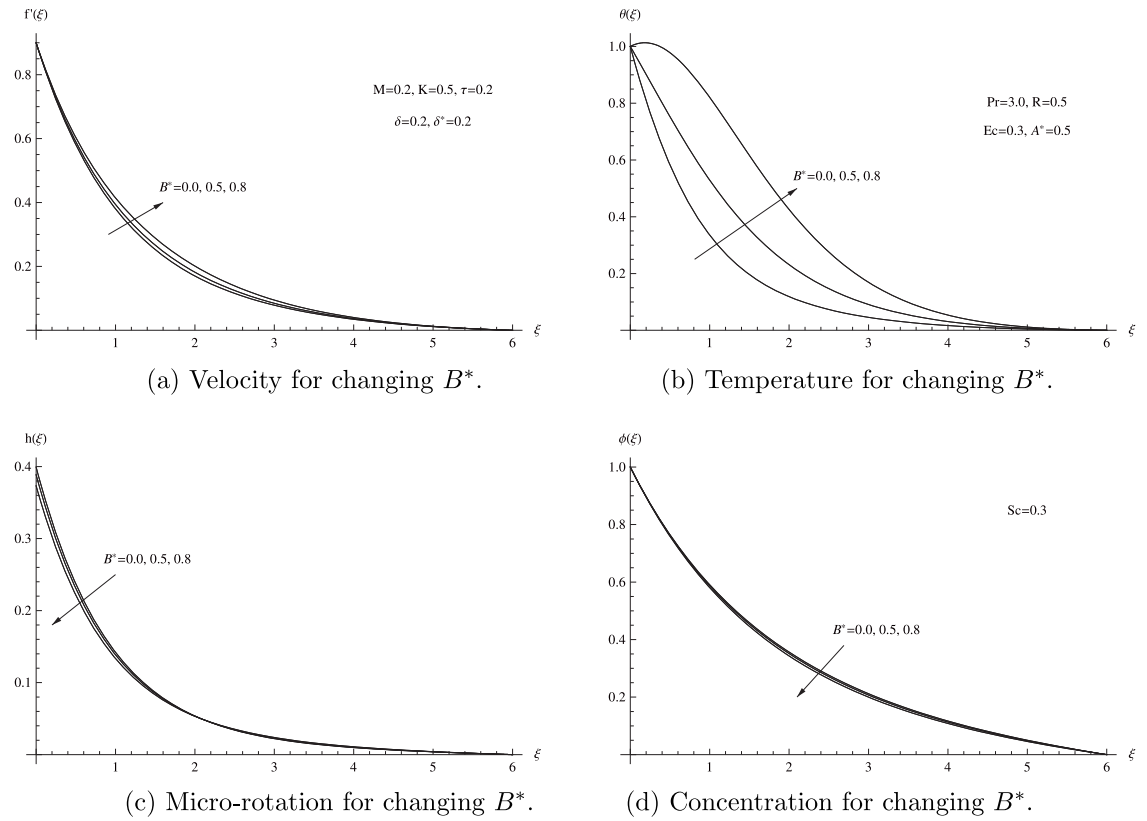

(a) Velocity for changing B^*. (b) Temperature for changing B^*.

(c) Micro-rotation for changing B^*. (d) Concentration for changing B^*.

Fig. 11.

Fig. 5(a, b, c, d) spectacle the impact of the thermal buoyancy parameter δ on the micropolar liquid velocity, temperature, angular momentum and concentration profiles. We perceived a fall in the micropolar liquid velocity profile for rising values of the thermal buoyancy parameter while the reverse trend is observed for the temperature, angular momentum and concentration profiles. This may be attributed to the fact that the increase of the values of thermal buoyancy parameter δ implies less expansion for the thermal boundary layer thickness.

Fig. 6(a, b, c, d) display the effect of the concentration buoyancy parameter δ^* on the micropolar liquid velocity, temperature, angular momentum and concentration profiles. We have an apparent reduction in the micropolar liquid velocity profile for rising values of the concentration buoyancy parameter while the reverse trend is observed for the temperature, angular momentum and concentration profiles. The reason behind this is the presence of the buoyancy force on the momentum equation, which takes action like stimulation force and as a result micro-rotation of fluid inside boundary layer decreases.

Fig. 7(a, b, c, d) are drafted to deliberate the variations in the micropolar liquid velocity, temperature, angular momentum and concentration distributions under the influence of Prandtl number Pr. From these graphs we found that boosting the values of the Prandtl number Pr declines the velocity and temperature profiles while the reverse trend is observed for the angular momentum and concentration profiles. This is in agreement with the physical fact that the thermal boundary layer thickness decreases with increasing Pr.

Fig. 8(a, b, c, d) demonstrate the impact of the thermal radiation parameter R on the micropolar liquid velocity, temperature, angular momentum and concentration profiles. It is manifest from these figures that the micropolar fluid velocity and temperature profiles enhance with the augmented values of thermal radiation parameter R while the reverse trend is observed for the angular momentum and concentration profiles. It was confirmed that the micropolar model especially in the presence of thermal radiation effect is applicable for small characteristic geometrical dimension of the flow.

Fig. 9(a, b, c, d) reveal the impact of the Eckert number Ec on the micropolar liquid velocity, temperature, angular momentum and concentration profiles. It is apparent from these figures that the micropolar fluid velocity

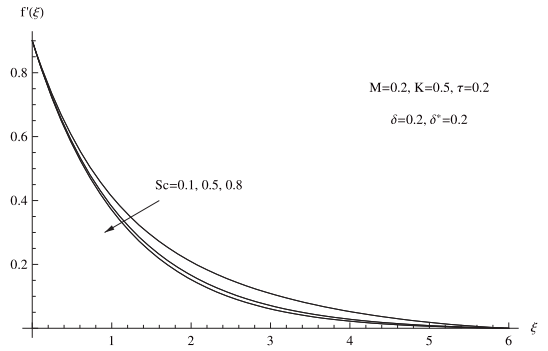

(a) Velocity for changing Sc.

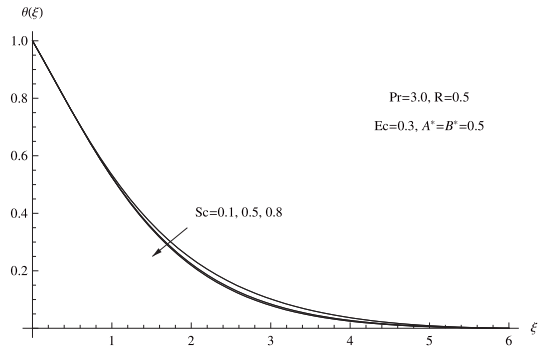

(b) Temperature for changing Sc.

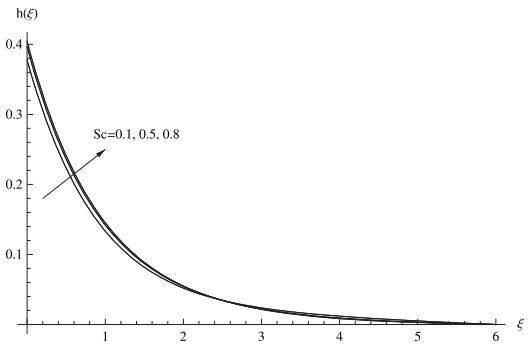

(c) Micro-rotation for changing Sc.

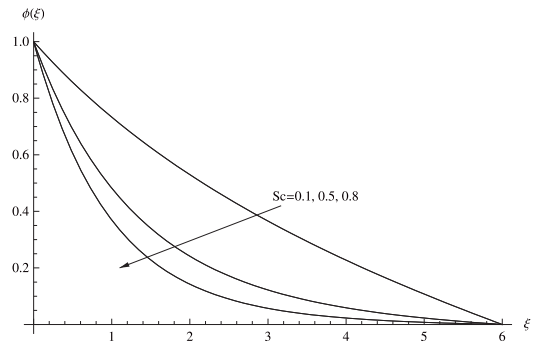

(d) Concentration for changing Sc.

Fig. 12.

and temperature profiles increase with the augmented values of the Eckert number Ec while the reverse trend is observed for the angular momentum and concentration profiles. Physically, it is observed that the case of cooling is more pronounced than that of the case of heating on the temperature profiles for small values of Eckert number Ec.

Fig. 10(a, b, c, d) disclose the effect of the space dependent internal heat source/sink parameter A^* on the micropolar liquid velocity, temperature, angular momentum and concentration profiles. It is evident from these figures that the micropolar fluid velocity and temperature profiles rise with the augmented values of the space dependent internal heat source/sink parameter A^* while the reverse tendency is observed for the angular momentum and concentration profiles.

Fig. 11(a, b, c, d) relate the effect of the temperature dependent internal heat source/sink parameter B^* on the micropolar liquid velocity, temperature, angular momentum and concentration profiles. It is manifest from these figures that the micropolar fluid velocity and temperature profiles increase with the augmented values of the temperature dependent internal heat source/sink parameter B^* while the reverse trend is observed for the angular momentum and concentration profiles.

Fig. 12(a, b, c, d) narrate the impact of the Schmidt number Sc on the micropolar liquid velocity, temperature, angular momentum and concentration profiles. It is evident from these figures that the micropolar fluid angular momentum profile increases with the augmented values of the Schmidt number Sc while the reverse trend is observed for the velocity, temperature and concentration profiles. It is observed that heavier species with great Schmidt number Sc is favorable to decrease the concentration profile as a result the concentration boundary layer thickness decreases.

5. Concluding remarks

We have examined the governing equations for an unsteady, incompressible MHD micropolar fluid with thermal radiation and heat source past a stretching (shirking) sheet and subjected to magnetic field. Fourth order predictor–corrector FDM method has been successfully used to solve numerically the proposed physical problem. The results are presented graphically with various system parameters in detail. Form the graphical representation, the following results are deduced from our study:

1. Micropolar fluid temperature, angular momentum and concentration profiles enhance with the augmented values of magnetic parameter while the reverse trend is observed for velocity profile;
2. Micropolar liquid velocity, temperature and angular momentum profiles are enhanced with the boost values of micropolar parameter while the reverse trend is observed for concentration profile;
3. Micropolar liquid velocity, temperature, angular momentum and concentration distributions are reduced for an escalation in the unsteadiness parameter;
4. Micropolar liquid velocity profile has rising values of the thermal buoyancy parameter while the reverse trend is observed for the temperature, angular momentum and concentration profiles;
5. Reduction in the micropolar liquid velocity profile for rising values of the concentration buoyancy parameter while the reverse trend is observed for the temperature, angular momentum and concentration profiles;
6. Prandtl number declines the velocity and temperature profiles while the reverse trend is observed for the angular momentum and concentration profiles;
7. Micropolar fluid velocity and temperature profiles are enhanced with the augmented values of thermal radiation parameter while the reverse trend is observed for the angular momentum and concentration profiles;
8. The micropolar fluid velocity and temperature profiles increase with the augmented values of the Eckert number while the reverse trend is observed for the angular momentum and concentration profiles;
9. Micropolar fluid velocity and temperature profiles increase with the augmented values of the temperature dependent internal heat source/sink parameter while the reverse trend is observed for the angular momentum and concentration profiles;
10. Micropolar fluid angular momentum profile increases with the augmented values of the Schmidt number while the reverse trend is observed for the velocity, temperature and concentration profiles.

Acknowledgments

The authors wish to express their sincere thanks to the reviewers for the valuable comments and suggestions.

References

[1] M. Abd El-Aziz, Mixed convection flow of a micropolar fluid from an unsteady stretching surface with viscous dissipation, J. Egyptian Math. Soc. 21 (2013) 385–394.
[2] Reda G. Abdel-Rahman, A.M. Megahed, Lie group analysis for a mixed convective flow and heat mass transfer over a permeable stretching surface with Soret and Dufour effects, J. Mech. 30 (2014) 67–75.
[3] S. Ahmadreza, A.A. Jafarian, A.S. Saedi, K. Hosseinzadeh, D.D. Ganji, Hydrothermal analysis of non-Newtonian second grade fluid flow on radiative stretching cylinder with Soret and Dufour effects, Case Stud. Therm. Eng. 13 (2019) 100384, 1-13.
[4] F. Aman, A. Ishak, I. Pop, MHD Stagnation point flow of a micropolar fluid toward a vertical plate with a convective surface boundary condition, Bull. Malays. Math. Sci. Soc. 36 (4) (2013) 865–879.
[5] M.A.E. Aziz, Viscous dissipation effect on mixed convection flow of a micropolar fluid over an exponentially stretching sheet, Can. J. Phys. 87 (2009) 359–368.
[6] A.A. Bakr, A.J. Chamkha, Oscillatory free convection of a micropolar rotating fluid on a vertical plate with variable heat flux and thermal radiation, Heat Transf. Res. 48 (2017) 139–159.
[7] R. Bhargava, L. Kumar, H.S. Takhar, Finite element solution of mixed convection micropolar fluid driven by a porous stretching sheet, Internat. J. Engrg. Sci. 41 (2003) 2161–2178.
[8] K. Bhattacharyya, S. Mukhopadhyay, G.C. Layek, I. Pop, Effects of thermal radiation on micropolar fluid flow and heat transfer over a porous shrinking sheet, Int. J. Heat Mass Transfer 55 (2012) 2945–2952.
[9] J. Chen, C. Liang, J.D. Lee, Theory and simulation of micropolar fluid dynamics, Proc. Inst. Mech. E, J. Nanoeng. Nanosyst. 224 (2010) 31–39.
[10] R. Derakhshan, S. Ahmadreza, K. Hosseinzadeh, M. Nimafar, D.D. Ganji, Hydrothermal analysis of magneto hydrodynamic nanofluid flow between two parallel by AGM, Case Stud. Therm. Eng. 14 (2019) 1–11.
[11] A. Desseaux, N.A. Kelson, Flow of a micropolar fluid bounded by a stretching sheet, ANZIAM J. 42 (2003) C536–C560.

[12] Feng Gao, X.J. Yang, F.Z. Yu, Exact traveling wave solutions for a new non-linear heat transfer equation, Therm. Sci. 21 (4) (2016) 1833–1838.
[13] M. Gholinia, S. Gholinia, K. Hosseinzadeh, D.D. Ganji, Investigation on ethylene glycol nano fluid flow over a vertical permeable circular cylinder under effect of magnetic field, Results Phys. 9 (2018) 1525–1533.
[14] M. Gholinia, K. Hosseinzadeh, H. Mehrzadi, D.D. Ganji, A.A. Ranjbar, Investigation of MHD eyring-Powell fluid flow over a rotating disk under effect of homogeneous-heterogeneous reactions, Case Stud. Therm. Eng. 13 (2019) 1–10.
[15] D. Gupta, L. Kumar, B. Singh, Finite element solution of unsteady mixed convection flow of micropolar fluid over a porous shrinking sheet, Sci. World J. 11 (2014) 362351, 1-11.
[16] T. Hayat, T. Javed, Z. Abbas, MHD Flow of a micropolar fluid near a stagnation point towards a non-linear stretching surface, Nonlin. Anal.: Real World Appl. 10 (2009) 1514–1526.
[17] T. Hayat, M. Khan, A.K. Tufail, I.K. Muhammad, Entropy generation in Darcy-forchheimer bidirectional flow of water-based carbon nanotubes with convective boundary conditions, J. Molecular Liquids 265 (2018) 12–26.
[18] T. Hayat, F. Muhammad, A. Alsaedi, A. Falleh, Impact of Cattaneo-Christov heat flux in the flow over a stretching sheet with variable thickness, AIP Adv. 5 (8) (2015) 1–12, http://dx.doi.org/10.1063/1.4929523.
[19] T. Hayat, A. Salman, M. Khan, A. Alsaedi, Modeling and analyzing flow of third grade nanofluid due to rotating stretchable disk with chemical reaction and heat source, Phys. Rev. B 537 (2018) 131–145.
[20] T. Hayat, A.K. Waleed, A. Alsaedi, M. Khan, Squeezing flow of second grade liquid subject to non-fourier heat flux and heat generation/absorption, Colloid Polym. Sci. 295 (4) (2017) 12–31.
[21] T. Hayata, S. Farooq, B. Ahmad, A. Alsaedi, Homogeneous-heterogeneous reactions and heat source/sink effects in MHD peristaltic flow of micropolar fluid with Newtonian heating in a curved channel, J. Mol. Liq. 223 (2016) 469–488.
[22] K. Hosseinzadeh, A. Asadi, A.R. Mogharrebi, K. Javad, M. Seyedmohammad, D.D. Ganji, Entropy generation analysis of (CH2OH)2 containing CNTs nanofluid flow under effect of MHD and thermal radiation, Case Stud. Therm. Eng. 14 (2019) 1–13.
[23] K. Hosseinzadeh, M. Gholinia, B. Jafari, A. Ghanbarpour, H. Olfian, D.D. Ganji, Nonlinear thermal radiation and chemical reaction effects on maxwell fluid flow with convectively heated plate in a porous medium, Heat Transfer-Asian Res. 48 (2) (2019) 744–759.
[24] K. Hosseinzadeh, A.R. Mogharrebi, A. Asadi, M. Paikar, D.D. Ganji, Effect of fin and hybrid nano-particles on solid process in hexagonal triplex latent heat thermal energy storage system, J. Molecular Liquids 300 (15) (2020) 112347.
[25] K.L. Hsiao, Heat and mass transfer for micropolar flow with radiation effect past a nonlinearly stretching sheet, Heat Mass Transfer 46 (4) (2010) 413–419.
[26] F.S. Ibrahim, A.M. Elaiw, A.A. Bakr, Influence of viscous dissipation and radiation on unsteady MHD mixed convection flow of micropolar fluids, Appl. Math. Inform. Sci. 2 (2) (2008) 143–162.
[27] F.S. Ibrahim, A.M. Elaiw, A.A. Bakr, Influence of viscous dissipation and radiation on unsteady MHD mixed convection flow of micropolar fluids, Appl. Math. Inform. Sci. 2 (2) (2008) 143–162.
[28] A. Ishak, Y.Y. Lok, I. Pop, Stagnation-point flow over a shrinking sheet in a micropolar fluid, Chem. Eng. Commun. 197 (2010) 1417–1427.
[29] R.N. Jat, S. Vishal, R. Dinesh, MHD Flow and heat transfer near the stagnation point of a micropolar fluid over a stretching surface with heat generation/ absorption, Indian J. Pure Appl. Phys. 51 (2013) 683–689.
[30] M.I. Khan, M. Waqas, T. Hayat, A. Alsaedi, A comparative study of casson fluid with homogeneous-heterogeneous reactions, J. Colloid Interface Sci. 498 (15) (2017) 85–90.
[31] Y.J. Kim, A.G. Fedorov, Transient mixed radiative convection flow of micropolar fluid past a moving semi-infinite vertical porous plate, Int. J. Heat Mass Transfer 46 (2013) 1751–1758.
[32] R. Madiha, M. Khan, T. Hayat, M.K. Imran, Entropy generation in flow of ferromagnetic liquid with nonlinear radiation and slip condition, J. Molecular Liquids 276 (2019) 1–14.
[33] M.A.A. Mahmoud, A.M. Megahed, Non-uniform heat generation effects on heat transfer of a non-Newtonian fluid over a non-linearly stretching sheet, Meccanica 47 (2012) 1131–1139.
[34] A.M. Megahed, MHD Viscous Casson fluid flow and heat transfer with second-order slip velocity and thermal slip over a permeable stretching sheet in the presence of internal heat generation/absorption and thermal radiation, Eur. Phys. J. Plus 130 (81) (2015) 1–15.
[35] S.R Mishra, J. Mohanty, J.K. Das, Free convective flow, heat and mass transfer in a micropolar fluid over a shrinking sheet in the presence of a heat source, J. Eng. Phys. Thermophys. 91 (4) (2018) 983–990.
[36] A.A. Mostafa, Shimaa, M.E. Waheed, MHD Flow and heat transfer of a micropolar fluid over a stretching surface with heat generation (absorption) and slip velocity, J. Egypt. Math. Soc. 20 (2012) 20–27.
[37] W. Muhammad, J. Shagufta, T. Hayat, M.K. Ijaz, A. Ahmed, Modeling and analysis for magnetic dipole impact in nonlinear thermally radiating Carreau nanofluid flow subject to heat generation, J. Magn. Magn. Mater. 485 (1) (2019) 197–204.
[38] W. Muhammed, M.S. Sher, T. Hayat, M. Khan, Simulation of magnetohydrodynamics and radiative heat transportation in convectively heated stratified flow of Jeffrey nanomaterial, J. Phys. Chem. Solids 133 (2019) 1–10.
[39] R. Nazar, N. Amin, D. Filip, I. Pop, Stagnation point flow of a micropolar fluid towards a stretching sheet, Int. J. Nonlin. Mech. 39 (2004) 1227–1235.
[40] D. Pal, S. Chatterjee, Heat and mass transfer in MHD non-darcian flow of a micropolar fluid over a stretching sheet embedded in a porous media with non-uniform heat source and thermal radiation, Commun. Nonlinear Sci. Numer. Simul. 15 (2010) 1843–1857.
[41] B.C. Prasannakumara, B.J. Gireesha, P.T. Manjunath, Melting phenomenon in MHD stagnation point flow of dusty fluid over a stretching sheet in the presence of thermal radiation and non-uniform heat source/sink, Int. J.Comput. Meth. Eng. Sci. Mech. 16 (2015) 265–274.
[42] S. Qayyum, T. Hayat, M.I. Khan, M.I. Khan, A. Alsaedi, Optimization of entropy generation and dissipative nonlinear radiative Von Karman's swirling flow with Soret and Dufour effects, J. Molecular Liquids 262 (2018) 261–274.

[43] M.M. Rahman, M.A. Sattar, Magnetohydrodynamic convective flow of a micropolar fluid past a continuously moving vertical porous plate in the presence of heat generation/absorption, J. Heat Transfer 128 (2006) 142–152.
[44] C.S.K Raju, N. Sandeep, C. Sulochana, V. Sugunamma, Effects of aligned magneticfield and radiation on the flow of ferrofluids over a flat plate with non-uniform heat source/sink, Inter. J. Sci. Eng. 8 (2) (2015) 151–158.
[45] M. Ramzan, M. Farooq, T. Hayat, Jae Dong Chunge, Radiative and joule heating effects in the MHD flow of a micropolar fluid with partial slip and convective boundary condition, J. Mol. Liq. 221 (2016) 394–400.
[46] A. Raptis, Boundary layer flow of a micropolar fluid through porous medium, J. Porous Media 3 (2000) 95–97.
[47] M.M. Rashidi, S.A. Mohimanian, S. Abbasbandy, Analytic approximate solutions for heat transfer of a micropolar fluid through a porous medium with radiation, Commun. Nonlin. Sci. Numer. Simul. 16 (2011) 1874–1881.
[48] S. Sajad, N. Amin, K. Hosseinzadeh, D.D. Ganji, Hydrothermal analysis of MHD squeezing mixture fluid suspended by hybrid nanoparticles between two parallel plates, Case Stud. Therm. Eng. 20 (2020) 1–14.
[49] M.D Shamshuddin, S.R Mishra, O.A Beg, A. Kadir, Unsteady reactive magnetic radiative micropolar flow, heat and mass transfer from an inclined plate with joule heating: a model for magnetic polymer processing, Proc. Inst. Mech. Eng. C 233 (4) (2018) 1246–1261.
[50] S. Shaw, P.K. Kameswaran, P. Sibanda, Homogeneous-heterogeneous reactions in micropolar fluid flow from a permeable stretching or shrinking sheet in a porous medium, Bound. Value Probl. 77 (2013) http://dx.doi.org/10.1186/1687-2770-2013-77.
[51] K. Singh, M. Kumar, Effects of thermal radiation on mixed convection flow of a micropolar fluid from an unsteady stretching surface with viscous dissipation and heat generation/absorption. Int. J. Chem. Eng. (2016), 8190234, p. 10.
[52] d. Srinivasacharya, C.H. Ram Reddy, Soret and dufour effects on mixed convection in a non-Darcy porous medium saturated with micropolar fluid, Nonlin. Anal.: Model.Control 16 (2011) 100–115.
[53] Q. Sumaira, M. Khan, T. Hayat, A. Alsaedi, Entropy generation in dissipative flow of Williamson fluid between two rotating disks, Int. J. Heat Mass Transfer 127 (2018) 933–942.
[54] N.A. Yacob, A. Ishak, I. Pop, Melting heat transfer in boundary layer stagnation-point flow towards a stretching/shrinking sheet in a micropolar fluid, Comput. Fluids 47 (2011) 16–21.
[55] X.J. Yang, A new integral transform method for solving steady heat-transfer problem, Therm. Sci. 20 (3) (2016) S639–S642.
[56] X.J. Yang, A new integral transform with an application in heat-transfer problem, Therm. Sci. 20 (3) (2016) S677–S681.
[57] X.J. Yang, A new integral transform operator for solving the heat-diffusion problem, Appl. Math. Lett. 64 (2017) 193–197.
[58] X.J. Yang, New integral transforms for solving a steady heat transfer problem, Thermal Science 21 (2017) S79–S87.
[59] X.J. Yang, Feng Gao, A new technology for solving diffusion and heat equations, Therm. Sci. 21 (1A) (2016) 133–140.
[60] X.J. Yang, Y. Yugui, C. Carlo, Mingzheng Zhu, A new technique for solving the 1-D Burgers equation, 21, (2017), S129-S136.
[61] K. Zaimi, A. Ishak, Stagnation-point flow and heat transfer over a nonlinearly stretching/shrinking sheet in a micropolar fluid, Abstr. Appl. Anal. 2014 (2014) 261630,6p, 1-9.
[62] M.R. Zangooee, K. Hosseinzadeh, D.D. Ganji, Hydrothermal analysis of MHD nanofluid (TiO2-GO) flow between two radiative stretchable rotating disks using AGM, Case Stud. Therm. Eng. 14 (2019) 1–13.